Life Sciences 273 (2021) 119300

Contents lists available at ScienceDirect

Life Sciences

journal homepage: www.elsevier.com/locate/lifescie

Early differences in membrane properties at the neuromuscular junctions of ALS model mice: Effects of 25-hydroxycholesterol

Guzel F. Zakyrjanova [a,b], Arthur R. Giniatullin [c], Kamilla A. Mukhutdinova [b], Eva A. Kuznetsova [a], Alexey M. Petrov [a,b,*]

[a] Laboratory of Biophysics of Synaptic Processes, Kazan Institute of Biochemistry and Biophysics, Federal Research Center "Kazan Scientific Center of RAS", 2/31 Lobachevsky Street, box 30, Kazan 420111, Russia
[b] Institute of Neuroscience, Kazan State Medial University, 49 Butlerova Street, Kazan, 420012, Russia
[c] Department of Normal Physiology, Kazan State Medial University, 49 Butlerova Street, Kazan 420012, Russia

ARTICLE INFO

Keywords:
Amyotrophic lateral sclerosis
Ceramide
25-Hydroxycholesterol
Neuromuscular junction
Lipid rafts
Reactive oxygen species

ABSTRACT

Aims: Plasma hyperlipidemia is a protective factor in amyotrophic lateral sclerosis (ALS) while cholesterol-lowering drugs aggravate the pathology. We hypothesize that this phenomenon can be linked with membrane lipid alterations in the neuromuscular junctions (NMJs) occurring before motor neuron loss.
Methods: Neurotransmitter release in parallel with lipid membrane properties in diaphragm NMJs of SOD1G93A (mSOD) mice at nine weeks of age (pre-onset stage) were assessed.
Key findings: Despite on slight changes in spontaneous and evoked quantum release of acetylcholine, extracellular levels of choline at resting conditions, an indicator of non-quantum release, were significantly increased in mSOD mice. The use of lipid-sensitive fluorescent probes points to lipid raft disruption in the NMJs of mSOD mice. However, content of cholesterol, a key raft component was unchanged implying another pathway responsible for the loss of raft integrity. In the mSOD mice we found marked increase in levels of raft-destabilizing lipid ceramide. This was accompanied by enhanced ability to uptake of exogenous ceramide in NMJs. Acute and chronic administration of 25-hydroxycholesterol, whose levels increase due to hypercholesterolemia, recovered early alterations in membrane properties. Furthermore, chronic treatment with 25-hydroxycholesterol prevented increase in ceramide and extracellular choline levels as well as suppressed lipid peroxidation of NMJ membranes and fragmentation of end plates.
Significance: Thus, lipid raft disruption likely due to ceramide accumulation could be early event in ALS which may trigger neuromuscular abnormalities. Cholesterol derivative 25-hydroxycholesterol may serve as a molecule restoring the membrane and functional properties of NMJs at the early stage.

1. Introduction

The initial events that trigger pathological processes occur before the manifestation of neurodegenerative disorders. Determination of such events is essential for understanding the pathogenesis and development of new strategies for disease therapy. Amyotrophic lateral sclerosis (ALS) is a non-curable disorder characterized by muscle denervation and massive death of motor neurons at late stages. Ultimately, respiratory failure causes lethality in ALS patients [1]. One of widely used model of ALS is a mouse overexpressing the human mutant copper/zinc superoxide dismutase 1, SOD1(G93A). Numerous studies pointed to dying-back pathology in this model, when muscle denervation occurs before motor neuron loss [1–7]. A similar pattern was found in ALS patients [1,2,8], suggesting that early alterations in neuromuscular junctions (NMJs) can greatly contribute to neurodegeneration. Along the same lines, therapeutic targeting only soma of motor neurons cannot rescue

Abbreviations: ACh, acetylcholine; AChE, acetylcholinesterase; ALS, amyotrophic lateral sclerosis; BODIPY-Cer, BODIPY-ceramide; Cer, ceramide; CTxB, cholera toxin subunit B; Chol, cholesterol; CSF, cerebrospinal fluid; EPC, end plate current; 25HC, 25-hydroxycholesterol; NMJ, neuromuscular junction; nAChR, nicotinic ACh receptor; MEPC, miniature EPC; mSOD, mutant copper/zinc superoxide dismutase 1; ROS, reactive oxygen species; VAPB, vesicle-associated membrane protein-associated protein B; WT, wild type.

* Corresponding author at: Institute of Neuroscience, Kazan State Medial University, 49 Butlerova Street, Kazan 420012, Russia.
E-mail address: alexey.petrov@kazangmu.ru (A.M. Petrov).

https://doi.org/10.1016/j.lfs.2021.119300
Received 5 December 2020; Received in revised form 13 February 2021; Accepted 25 February 2021
Available online 2 March 2021

the mutant SOD1 mice [1,6,9,10] and muscle-specific overexpression of the mutant SOD1 is enough to provoke ALS signs and motor neuron death [11,12].

Currently, there is only scarce information regarding early changes in NMJs at pre-onset stage of ALS. At this phase, an increase in evoked acetylcholine (ACh) release was found in diaphragm of SOD1(G93A) mice [13]. This was accompanied by disruption of crosstalk between adenosine A_1 and A_2 receptors which are important for suppression of ACh exocytosis [14]. Furthermore, an increase in ACh-mediated activation of muscarinic receptor was responsible for enhanced Ca^{2+} responses of peri-synaptic Schwann cell to synaptic activity in SOD1 (G37R) mice at pre-onset stage [15]. Increased expression of NMJ-destabilizing factors and negative regulator of neurite outgrowth CRMP4a as well as appearance of deficit in TrkB signaling essential for maintenance of synaptic contacts were observed in muscle of pre-onset stage SOD1(G93A) mice [16–18].

Intriguingly, hypolipidemia is present in pre-onset stage SOD1 (G93A) mice [19]. Also, accumulation of ceramide (Cer) in spinal cord preceded the phenotype in SOD1(G93A) mice [20]. These data are in agreement with abnormal lipid metabolism in ALS patients and that hyperlipidemia is negatively correlated with severity of ALS [20–24]. Probably, upregulation of plasma cholesterol (Chol) could affect membrane properties thereby ameliorating the progression of ALS. This is consistent with ability of Chol-like and raft-stabilizing molecule olesoxime to exert protective properties in ALS models [25–27]. Furthermore, neuronal-specific overexpression of raft-organizing protein caveolin-1 increased raft localization of TrkB, improved NMJ function and extended survival of SOD1(G93A) mice [28]. Lipid rafts can modulate signaling dependent on TrkB and adenosine A_2 receptors, thereby protecting neurons from mutant SOD1-induced toxicity [29]. It is tempting to propose that changes in membrane properties in NMJs could occur early in ALS, thereby interfering with “normal” signaling and contributing to pathological alterations.

In the present work, we examined the differences in membrane properties at diaphragm NMJs in parallel with tracking for neurotransmission in SOD1G93A mice at nine weeks of age (pre-onset stage). Additionally, effects of acute and chronic pretreatment with 25-hydroxycholesterol (25HC), whose levels were found to be changed in serum of ALS patients [30,31], were evaluated.

2. Methods

2.1. Animals

Experiments were performed on isolated phrenic nerve-diaphragm preparations from nine-week-old mice of both sexes. The low-expressing transgenic $SOD1^{G93A}$ mice (B6SJL-Tg(SOD1-G93A)^{dl}1Gur/J strain; stock # 002300, purchased from The Jackson Laboratory) were maintained as a hemizygous line in an SPF-breeding facility (Bioresource Collection of the Branch of RAS Institute of Bioorganic Chemistry, Moscow Region). Only F1 generation of the hemizygous mice was used after crossing Tg(SOD1-G93A)dl1Gur/J hemizygous male mice with non-transgenic wild-type B6SJL female mice (The Jackson Laboratory). Gender-matched B6SJL littermates served as a wild type (WT) control. The onset of the disease manifestation is delayed in this SOD1G93A genotype compared to the original high copy number (SOD1 G93A)1Gur strain and there are no ALS signs until 3 months of age [32]. This mouse model was used to focus specifically on early differences. These mice become paralyzed, at least, in one limb beginning at 6–7 months of age and life expectancy is usually 4 to 6 weeks beyond the onset of paralysis [32,33]. Mutant and WT mice were housed four per ventilated cage under standard conditions (temperature: 20–24°C; humidity: 30–70%) and maintained in a 12:12-h light-dark cycle with food and water *ad libitum*. Nine-week-old animals were anesthetized (intraperitoneal injection of sodium pentobarbital; 40 mg/kg) before decapitation with a guillotine. The experimental protocol met the requirements of the EU Directive 2010/63/EU and was approved by the Bioethics Committees of Kazan Medical University. This study conforms to the European Convention for the Protection of Vertebrate Animals used for Experimental and other Scientific Purposes. Experimenters were not blinded regarding to mouse genotype or treatments. The used assessments were quantitative and data analysis should not be affected by investigators’ bias as all data were used and outliers were not excluded.

2.2. Solution and chemicals

The diaphragm muscle with phrenic nerve stubs was quickly excised immediately after euthanasia. The diaphragm was dissected into two hemidiaphragms with individual nerve stub. The cut end of phrenic nerve was loosely drawn into a suction pipette with stimulating electrodes. Hemidiaphragms were attached to the bottom of a Sylgard-lined chamber (volume, 5 ml), which was continuously perfused at 5 $ml \cdot min^{-1}$ with carbogen-saturated physiological saline containing (in mM): 129.0 NaCl, 5.0 KCl, 2.0 $CaCl_2$, 1.0 $MgSO_4$, 1.0 NaH_2PO_4, 20.0 $NaHCO_3$, 11.0 glucose and 3.0 HEPES. 25HC (Sigma) was dissolved in DMSO and then diluted in physiological solution to give a final concentration. The final concentration of DMSO in the working solution was extremely low, below 0.0001% (*v*/v). DMSO (0.001%) by itself did not alter any of the estimated parameters, consistent with our previous data [26,34,35], and the results from DMSO controls were pooled together with controls. Basal concentration of 25HC in plasma is low (˂ 0.1 μM) and can increase up to 1 μM in response to induction of inflammatory response [36,37]. So, the concentration of 1 μM and corresponding dose (0.4 mg/kg, intraperitoneal injection) were chosen for acute and chronic administration of 25HC, respectively. Acute application of 25HC lasted 1.5 h before the onset of labeling with fluorescent indicators. Long-term treated mice received intraperitoneal injections of 25HC (0.4 mg/kg) in physiological saline (total volume – 0.2 ml) once per four days during one month (a total of eight injections), while control groups of animals were injected with the same solution without 25HC. The chronic treatment with 25HC lasted from 4.5 to 9 weeks of age. The implications of treating juvenile mice were studied to reveal the influence of 25HC on appearance of membrane-related abnormalities in mSOD mice at early pre-onset stage.

2.3. Electrophysiological recording

Postsynaptic signals, specifically end-plate currents (EPCs) and miniature EPC (MEPCs) were recorded using two-electrode voltage clamp technique as described previously [38,39]. Briefly, intracellular glass microelectrodes (resistance of 3-5 MΩ and ~ 1 μm tip diameter) were filled with 2.5 M KCl and placed in synaptic zone with interelectrode distance of ~200–300 μm. The muscle fibers were cut transversely to block contractions despite the normal level of quantal release of ACh. The cutting procedure does not produce significant changes in cable properties and enables long-lasting recording of postsynaptic currents [40]. The potential of the muscle fibers was kept at −45 mV; leak current was in the range of 10–30 nA. The phrenic nerve was stimulated with a suction electrode by single stimuli (at 0.5 Hz) or 20-Hz train of 0.1-ms suprathreshold pulses. The postsynaptic responses were digitized at 50 kHz and analyzed off-line using *Elph* software [41]. Recording equipment consisted of an Axoclamp 900 A amplifier (Molecular devices, USA) and LA II digital I/O board (Pushino, Russia). MEPPs or EPPs (at 0.5 Hz) were recorded from 25 to 30 different muscle fibers. The data from individual muscle fibers were then pooled to obtain average values of MEPP and EPP parameters in the muscle. These average values are presented in figures.

2.4. Choline assay

Choline levels were estimated as described [42–44]. Amplex® Red

Acetylcholine Assay Kit (Molecular Probes) was used to assess the choline/ACh released in diaphragm with active endogenous acetylcholinesterase (AChE). Briefly, freshly isolated muscles were incubated for short-term period (15 min) in physiological solution (0.4 ml) containing choline oxidase (EC 1.1.3.17, 1 U/ml), horseradish peroxidase (EC 1.11.1.7, HRP, 2 U/ml), and 400 μM Amplex® Red at 37C. The solution was continuously mixed by recirculating mechanism. The approach is based on the measurement of choline released due to hydrolysis of ACh by endogenous AChE in synaptic cleft. Choline oxidase breaks down choline to betaine and H_2O_2; then utilizing H_2O_2 HRP catalyzes oxidation of Amplex® Red reagent into a stable fluorescent compound resorufin. Additionally, total extracellular levels of ACh were assessed in the same conditions but with the addition of exogenous AChE (1 U/ml; E.C. 3.1.1.7.) into the reactive mixture. The exogenous AChE breaks residual non-hydrolyzed ACh (including the portion that evades enzymatic degradation by endogenous AChE). After 15-min incubation, the bathing solution was collected and stored at dark for 45 min before measurements of final resorufin signal (excitation at 535 nm and emission detection at 590 nm). For each measurement, we made a correction for non-specific signal caused by the endogenous H_2O_2 due to reactions other than choline oxidation. The levels of choline were determined from calibration curves, which were plotted as fluorescence at 590 nm *vs* increasing concentrations of ACh in presence of reagent mixture (plus exogenous 1 U/ml AChE). In some experiments, to saturate membrane with Chol, muscles were exposed to complexed MβCD-Chol (5 mM) for 15 min and then washed briefly [45,46] before measurements of choline.

2.5. Lipid assay in muscle tissue

Chol and Cer levels were analyzed as described [47]. Briefly, lipids were extracted from muscle homogenates by the Folch method. Chloroform extracts were spotted on HPTLC Silica gel 60 F254 plates (Merck, Germany) and developed in a solvent system of butanol:acetic acid: water (3:1:1). Plates were exposed to iodine vapor and scanned using video-densitometer (Sorbfil) at 254 nm. Quantitative analysis of Cer levels was performed with Sorbfil TLC Videodensitometer software. Chol content in the tissue homogenates was estimated using colorimetric enzymatic method (Vital test) according to manufacturer's instruction.

2.6. Hydroperoxide assay

Intracellular hydroperoxide content in muscle tissue was assessed with ferrous oxidation in xylenol orange (FOX1) as described [39,48]. This approach is based on peroxide-mediated oxidation of ferrous ions in the presence of xylenol orange; the later interacts with the resulting ferric ions to generate a blue–purple complex (maximum of absorbance at 540–580 nm). The levels of peroxides were calculated from calibration curve obtained with known concentrations of H_2O_2.

2.7. Fluorescence microscopy

Fluorescence was detected using a BX51WI microscope (Olympus) with a confocal DSU attachment, DIC-optics, objectives (UPLANSapo 60xw, LumPlanPF 100xw) and DP71 (Olympus) CCD camera. For image analysis Image^{Pro} software (Media Cybernetics) was used. The fluorescence was calculated in regions of interest as a mean fluorescence intensity in arbitrary units (a.u.). Fluorescence was recorded from 20 to 30 different NMJs/muscle fibers within each muscle from individual animal. The values obtained from the separate muscle fibers were then pooled to calculate average values of the fluorescence in the muscle/animal. The average values from individual animals were presented in the box plots.

Labeling with rhodamine-conjugated α-bungarotoxin (α-Btx), a specific marker of postsynaptic nicotinic ACh receptors (nAChRs), helped to identify the synaptic region. α-Btx (100 ng/ml, ThermoFisher) was added to the bathing solution for 15 min. α-Btx fluorescence was detected using excitation at 555/15 nm and 630/20 nm band-pass emission filter. Junctional fluorescence was determined in the α-Btx-positive region; extrajunctional signal was estimated in area (~200 μm^2) outside of the junctional membrane. Fluorescence of CTxB, BODIPY-ganglioside, BODIPY-ceramide (BODIPY-Cer) and 22-NBD-cholesterol was excited by a light of 488/10 nm; emission was recorded using band-pass filters (505–545 nm or 510–590 nm).

2.8. Lipid microenvironment-sensitive dyes

2.8.1. Cholera toxin subunit B (CTxB)

Lipid rafts were labeled with CTxB conjugated to AlexaFluor 488 (Molecular Probes). CTxB specifically binds with cluster of GM1 gangliosides mainly resided in the lipid rafts. Muscles were exposed for 20 min to physiological saline with CTxB (1 μg/ml); the samples were then washed for 30 min and visualized [45,46].

2.8.2. BODIPY FL C5-ganglioside GM1

To track ganglioside GM1 distribution in membranes, a green-fluorescent BODIPY FL C5-ganglioside GM1 complexed to bovine serum albumin (Molecular Probes) was used [26,47]. BODIPY-ganglioside GM1 was diluted in physiological solution. Muscles were incubated for 20 min with the fluorescent ganglioside GM1 (0.1 μM) and then washed for 30 min before recording of the fluorescence.

2.8.3. 22NBD-cholesterol

22-(N-(7-Nitrobenz-2-Oxa-1,3-Diazol-4-yl)Amino)-23,24-Bisnor-5-Cholen-3β-Ol (22NBD-cholesterol; Molecular Probes) is an environment-sensitive probe, whose fluorescence enhances in response to increase in membrane fluidity, *i.e.* membrane phase changes from a raft to non-raft fraction. Muscles were incubated for 20 min with 0.2 μM 22NBD-cholesterol in physiological saline and then perfused for 30 min with the dye-free physiological solution [26,45].

2.8.4. F2N12S

(A35137T, ThermoFisher) is a violet excitable fluorescent probe for detection of the loss of membrane ordering and (or) the plasma membrane asymmetry. This probe selectively binds to the outer leaflet of plasma membranes [49]. Samples were exposed to F2N12S (0.2 μM) for 5 min and then briefly perfused with dye-free physiological saline for 5 min. F2N12S fluorescence was recorded within 20 min using excitation at a 405/15 nm light and emission detection at 510/30 nm (green channel) and 585/30 nm (red channel). The ratio of R/G fluorescence was calculated. Decrease in membrane ordering and (or) asymmetry causes a decrease in the R/G ratio [49,50].

2.9. Uptake of Cer and Chol

For tracking of Cer incorporation into the plasma membranes and intracellular membranes, a green-fluorescent BODIPY™ FL C5-Cer complexed to bovine serum albumin (ThermoFisher) was used [50]. BODIPY-Cer was dissolved in physiological saline (final concentration of 0.1 μM). The preparations were perfused for $1^{1/2}$ h with BODIPY-Cer-containing (1 ml·min^{-1}) solution and then washed (at perfusion rate of 5 ml·min^{-1}) for $1^{1/2}$ h with the dye-free physiological saline to remove unbound fluorescent Cer. To test the ability to uptake Chol and 25HC, 25-(C4 TopFluor®) 25-OH cholesterol (BODIPY-cholesterol; Avanti) was applied. This probe has a similar behavior to Chol (partitioning in membrane, intracellular traffic and storage) and is translocated by oxysterol-binding proteins [51,52]. Muscles were exposed for 1.5 h with 1 μM 25-(C4 TopFluor) 25-OH cholesterol, then the dye was washed for $1^{1/2}$ h before recording of fluorescence. BODIPY (C4 TopFluor) fluorescence was excited by a light of 488/10 nm and emission was recorded using a 505–545 nm bandpass filter.

2.10. Lipid peroxidation assay

Image-iT sensor (BODIPY 581/591 C11 reagent) was used as a ratiometric indicator of lipid peroxidation (Molecular Probes). Upon membrane lipid peroxidation, fluorescence of the iT sensor shifts from red (590 nM) to green (510 nM), giving an indication of membrane lipid oxidation. Muscles were incubated with the dye (10 μM) for 30 min, rinsed with a physiological solution for 30 min. Then images were recorded using emission filters for fluorescein isothiocyanate and Texas Red. Intensities of green and red fluorescence were calculated and then converted into ratio between red and green signals [39,48].

2.11. Statistics

Statistical analysis was performed with Origin Pro software. There were no exclusions of outliers. Data are presented as mean ± SD; the sample size (n mice; the number of independent experiments on separate muscles from individual mice) and number of analyzed muscle fibers (if applicable) are indicated in each figure legend. Statistical significance of the difference between means was assessed by Mann–Whitney *U* test or a two-tailed, unpaired *t*-test. Statistical significance was defined as *P < 0.05, **P < 0.01 and ***P < 0.001.

3. Results

3.1. Electrophysiological characterization

MEPC frequency reflects a spontaneous neurotransmitter release from presynaptic nerve terminal while shape of MEPCs is mainly determined by properties of the postsynaptic nAChRs and activity of AChE in the synaptic cleft. In mSOD mice, frequency and amplitude of the MEPCs were higher than in WT. Rise and decay times of the MEPCs were lower in mSOD animals (Fig. 1A). These data suggest that slight increase in spontaneous release as well as alterations in postsynaptic nAChR functionality and (or) AChE activity can occur in mSOD mice at early stages.

Surprisingly, parameters of EPCs were not changed significantly, excluding EPC amplitude which was slightly higher in mSOD *vs* WT mice (Fig. 1B). This increase in the EPC amplitude was likely due to change in postsynaptic sensitivity rather than in evoked neurotransmission release. Since estimation of quantum content of EPCs by two approaches (namely, dividing of EPC on MEPC amplitudes and analysis of EPC amplitude variation [53]) indicated no changes in evoked neurotransmitter release in the NMJ of mSOD mice (Suppl. Fig. 1). Unchanged decay time of EPCs pointed to no marked differences in AChE activity in the neuromuscular junctions.

The nerve stimulation at 20 Hz caused a two-phase depression of neurotransmitter release (Fig. 1C): a fast reduction of EPC amplitude followed by a "plateau". In mSOD mice, after initial robust decrease and plateau EPC amplitude continued to reduce at a slow rate. Despite the

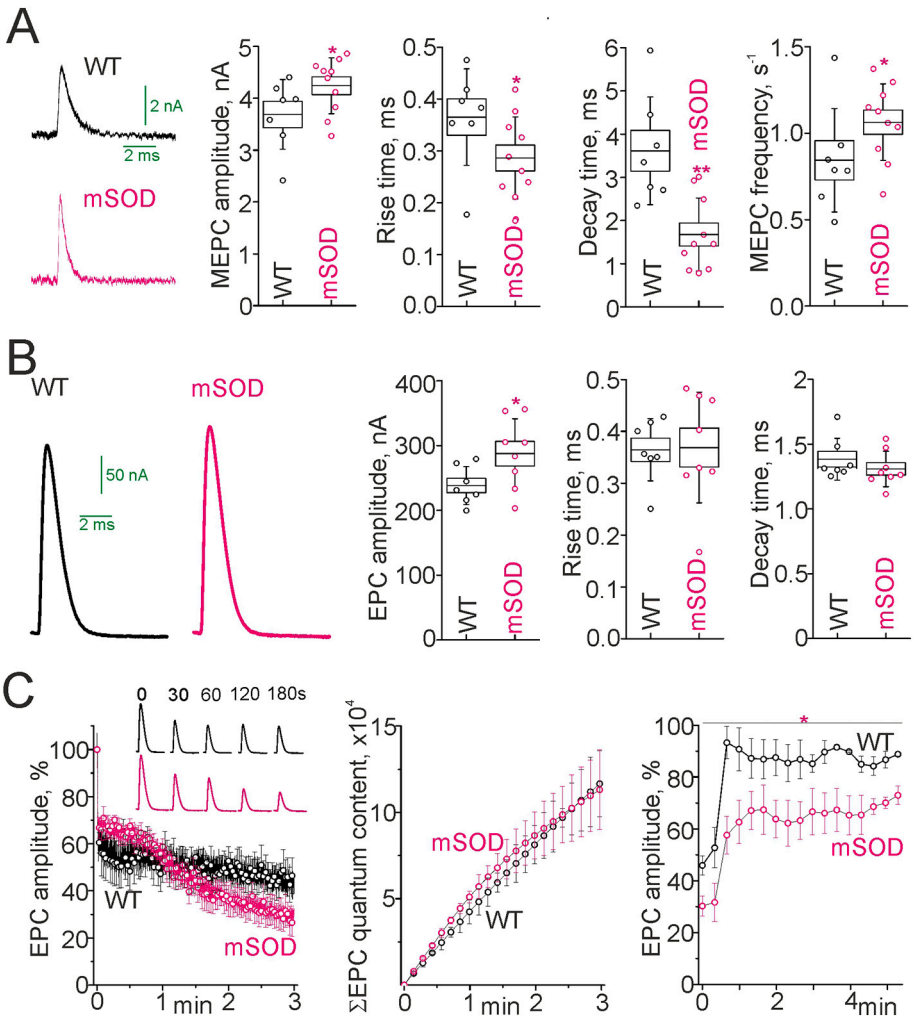

Fig. 1. Electrophysiological analysis of synaptic transmission in the NMJs of mSOD mice and WT mice. A – MEPCs and their parameters in WT and mSOD mice. Shown typical MEPCs and box plots indicating alterations of amplitude, rise and delay times, and frequency of MEPCs. $N = 7$ (204 muscle fibers) and 10 (277 muscle fibers) for WT and mSOD, respectively. B – EPCs at 0.5 Hz and their parameters. Shown representative EPCs and box plots illustrating amplitude, rise and decay times of EPCs. N = 7 (182 muscle fibers) and 8 (208 muscle fibers) for WT and mSOD, respectively. C – Effect of prolonged 20 Hz activity. Shown dynamics of EPC amplitude and cumulative quantum content during 20 Hz activity, and recovery of the EPC amplitude after 20-Hz stimulus train. In the last case, EPCs were evoked by 0.5 Hz stimulation. N = 7 and 8 mice for WT and mSOD curves, respectively. Data are represented as mean ± SD; *$P < 0.05$.

difference in kinetics of EPC amplitude rundown, estimation of cumulative neurotransmitter release pointed to the same number of quanta secreted for 3 min of 20 Hz stimulation in mSOD and WT mice. Only a recovery of the EPC amplitude after 20-Hz train was visibly slower in the mSOD compared to WT mice (Fig. 1C). Accordingly, there are no marked alterations in evoked neurotransmitter release in the mSOD mice, only additional stressing with the stimulation revealed a decreased ability to recovery the neurotransmitter release after the episode of 20 Hz activity.

3.2. Extracellular choline levels

At rest conditions a major portion of extracellular ACh originates from non-vesicular (non-quantum) secretion which is mediated by neurotransmitter transporters inserted into the presynaptic membrane [42,54,55]. In synaptic cleft ACh molecules are rapidly hydrolyzed by AChE, releasing acetate and choline. Extracellular levels of choline precisely reflect non-quantum ACh release in NMJs [42]. Hence, extracellular levels of choline, accumulated for 15-min period, were estimated. Surprisingly, extracellular choline content was markedly higher (by 43 ± 17%, $p = 0.0009$) in mSOD *vs* WT mice (Fig. 2A). Most modulators of neuromuscular transmission (ATP, glutamate, muscarinic agonists) suppress the non-quantal release in mammalian NMJs [55]. In contrast, even slight membrane cholesterol depletion can increase the non-vesicular ACh release due to increased activity of ACh transporter in the presynaptic membrane of the rat NMJs [42]. Accordingly, a potential reason for raise of extracellular choline might be membrane fluidity-related changes in the NMJs of mSOD mice. Consistent with this idea, saturation of membranes with exogenous Chol (using complexed MβCD-Chol; [45,56]) reduced extracellular choline content in mSOD mice to the control value, while Chol supplementation had no significant influence on choline levels in WT mice (Fig. 2A). It is tempting to suggest that changes in membrane properties of NMJs could occur early in ALS.

Residual ACh (non-hydrolyzed by endogenous AChE) was estimated in experiments with addition of exogenous AChE (Fig. 2B). In these experiments the levels of choline were on 37 ± 13% ($p = 0.0015$) higher than in conditions without addition of the exogenous AChE in WT mice. It means that ~37% of ACh escaped from endogenous AChE action. In the presence of exogenous AChE, the estimated levels of choline were higher (by 43 ± 15%, $p = 0.0022$) in mSOD mice *vs* WT mice and Chol supplementation decreased choline content in mSOD mice, whereas had no effect in WT mice (Fig. 2B). These results are consistent with data obtained without addition of exogenous AChE and point to increase in ACh release in the resting neuromuscular preparations. Note that a similar degree of the increase in choline levels, estimated without (Fig. 2A) and with the addition of exogenous AChE (Fig. 2B), suggests no significant difference in activity of endogenous AChE in mSOD mice compared to WT mice.

3.3. Differences in junctional and extrajunctional membrane properties

Fluorescent approaches allow to assess membrane properties selectively in junctional compartment of the living muscle fibers. To test hypothesis that alteration of the lipid rafts is early event in ALS, we used fluorescent-labeled CTxB, which selectively binds to GM1 ganglioside clusters mainly located in lipid rafts [57], and fluorescent ganglioside GM1, which preferentially inserts into the lipid ordered (raft) phase of the plasma membrane [26,58]. Staining of plasma membranes with CTxB was markedly lower in junctional regions (Fig. 3A) of mSOD mice compared to WT mice. In extrajunctional regions the CTxB fluorescence was not significant different ($p = 0.185$) in the mutant *vs* WT mice. The fluorescence of GM1 ganglioside was decreased in both junctional and extrajunctional membrane regions of mSOD mice (Fig. 3B). These data suggest that a decrease in lipid raft integrity could occur early in NMJs of mSOD mice.

NBD-cholesterol is an environment sensitive dye and elevation in membrane fluidity increases fluorescence of NBD-cholesterol incorporated into the plasma membranes [26,45,59]. In SOD mice the NBD-cholesterol fluorescence was significantly higher than in WT animals (Fig. 3C). Hence, an increment of membrane fluidly, *i.e.* disordering, may occur in the plasma membranes of SOD mice at the pre-onset stage. This is consistent with a proposed disturbance of membrane lipid-ordered phase (lipid rafts) in NMJs of mSOD mice.

To additionally test the differences in plasma membrane ordering, we used ratiometric probe F2N12S. Decrease in a ratio of red/green F2N12S fluorescence indicates an expansion of lipid-disordered phase and (or) loss of membrane asymmetry [50,60,61]. In mSOD mice, this ratio of F2N12S fluorescence decreased in junctional regions of the muscle (Fig. 3C). Thus, the use of four different dyes suggests a marked reduction of the lipid ordering (raft integrity) in junctional membrane at diaphragm muscle of the pre-onset stage mSOD mice.

3.4. Chol and Cer levels. Differences in uptake of fluorescent Cer

Chol is a dynamic glue for keeping components of lipid raft together and a regulator of membrane fluidity. Partial Chol depletion can cause lipid raft disruption in NMJs [45,46]. However, levels of Chol were similar in muscle homogenates from pre-onset stage mSOD and WT mice (Fig. 4A). Of course, this does not exclude that local Chol content in junctional compartment can be altered, because biochemical measurements show only total Chol in muscle tissue, containing mostly muscle fiber lipids.

Impaired Cer metabolism and its accumulation can contribute to

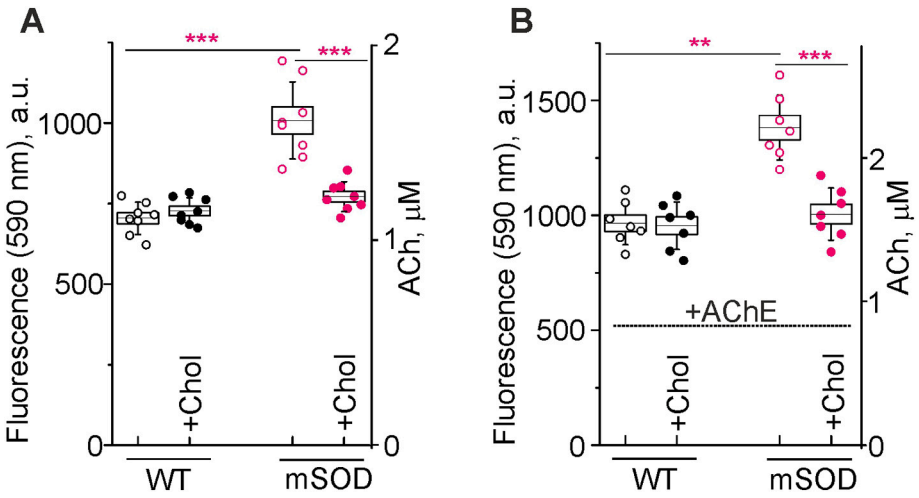

Fig. 2. Extracellular choline/ACh levels at rest conditions. A - shown choline fluorescence (at 590 nm; in a.u.) in the extracellular solution after 15-min incubation of the muscles from WT and mSOD mice. B – the same measurements in the presence of exogenous AChE that converts residual ACh (non-hydrolyzed by endogenous AChE) into choline. Some muscles were supplemented with Chol prior to onset of the 15-min incubation (+Chol). The fluorescence was compared to ACh calibration curve to evaluate the levels of ACh/choline (right Y axis). n = 7–8 mice for each group. Data are represented as mean ± SD; $^{**}P < 0.01$, $^{***}P < 0.001$.

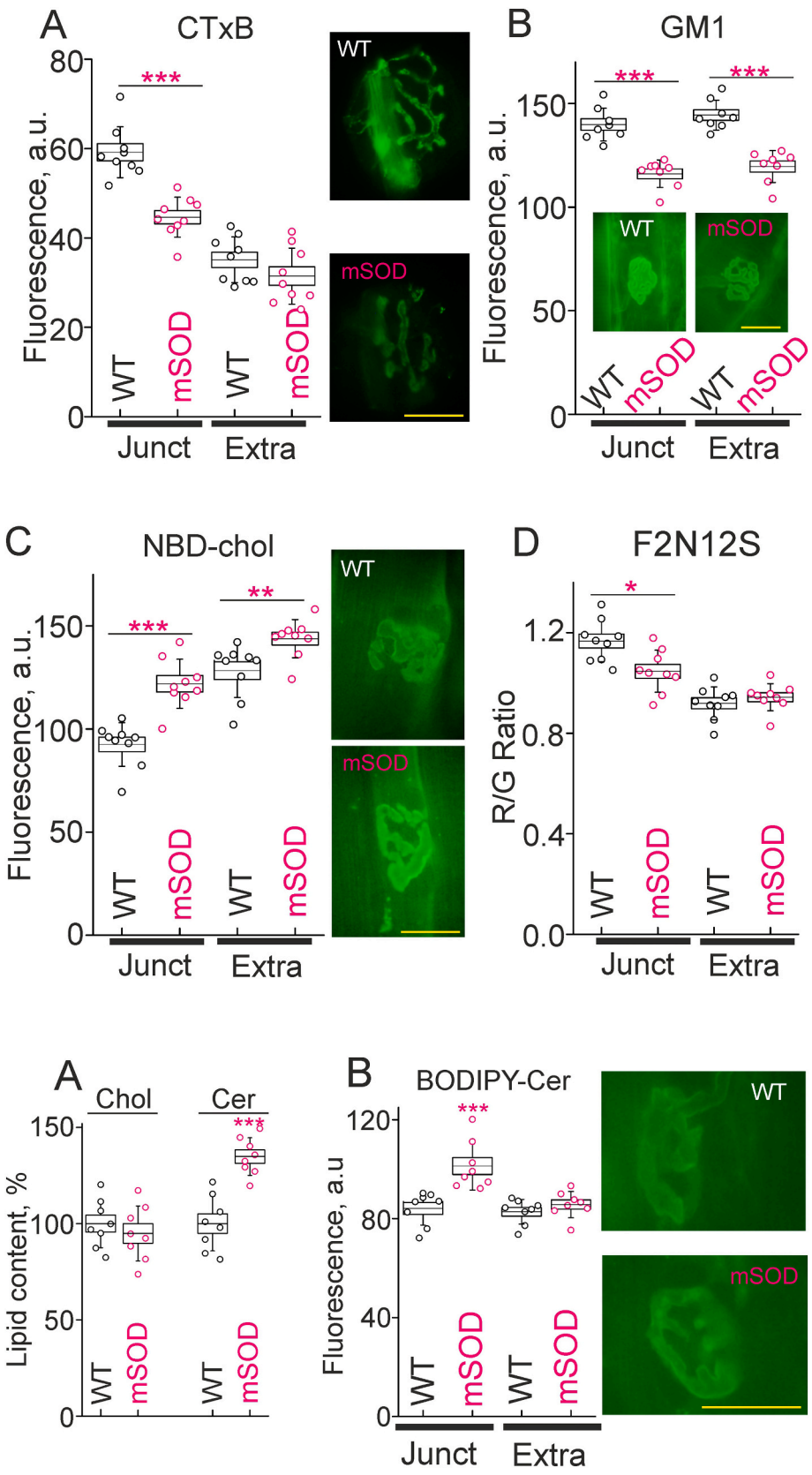

Fig. 3. Plasma membrane properties in junctional and extrajunctional regions. A – Labeling of lipid rafts with fluorescent CTxB. $N = 9$ mice per group (258 and 263 muscle fibers for WT and mSOD, respectively). B – Staining with fluorescent GM1 ganglioside targeting to lipid raft (ordering) phase. $N = 8$ mice per group (209 and 231 muscle fibers for WT and mSOD, respectively). C- Fluorescence of membrane fluidity-sensitive probe NBD-cholesterol. Increased fluorescence of the NBD-cholesterol points to an increase in membrane fluidity (*i.e.* decrease in lipid ordering). N = 9 mice per group (261 and 267 muscle fibers for WT and mSOD, respectively). A-B, histograms showing fluorescence (in a.u); and typical fluorescent images of junctional regions; scale bars – 20 μm. D - Ratio of red / green fluorescence of F2N12S dye, an indicator of membrane ordering and (or) asymmetry. N = 9 mice per group (202 and 214 muscle fibers for WT and mSOD, respectively). Data are represented as mean ± SD; $*P < 0.05$, $**P < 0.01$, $***P < 0.001$. (For interpretation of the references to colour in this figure legend, the reader is referred to the web version of this article.)

Fig. 4. Chol and Cer content. A – Relative levels of Chol and Cer in the muscle homogenates of WT and mSOD mice. N = 8 mice for each group. B – Uptake of fluorescent Cer. Left, fluorescence (in a.u.) in junctional and extrajunctional regions; right, representative fluorescent image of region containing junctional compartment, scale bar – 20 μm. N = 8 mice per group (192 and 208 muscle fibers for WT and mSOD, respectively). A, B - data are represented as mean ± SD; $***P < 0.001$.

lipid raft disturbance, synaptic dysfunction as well as metabolic dysregulation in skeletal muscles [47,50,62,63]. Cer content was higher in diaphragm muscle of mSOD compared to WT mice (Fig. 4A). In addition, use of BODIPY-Cer revealed its greater accumulation selectively in the junctional region of mSOD mice (Fig. 4 B). The fluorescent Cer formed hot-spots of the fluorescence within the synaptic zone in mSOD mice. This indicates on Cer accumulation in plasma membrane and intracellular membranes (endoplasmic reticulum and endosomes) in the NMJs.

Accordingly, increased Cer levels and its synaptic accumulation may occur in mSOD mice at early stage.

3.5. Influence of acute oxysterol application on membrane properties

Oxysterols can affect both properties of synaptic membranes and neuromuscular transmission [26,38,46]. Recent studies suggest an engagement in ALS of immune-related oxysterol 25HC, whose production is induced by various toll-like receptor ligands and interferons [30,31] as well as hypercholesterolemia and dietary Chol challenge [64,65]. Despite numerous important activities (anti-viral, cardioprotective, anticancer, regulation of Chol homeostasis) of 25HC, its role in ALS remains unknown.

Application of 25HC for 1.5 h did not change both staining with ganglioside GM1 (Fig. 5A) and fluorescence of NBD-cholesterol (Fig. 5B) in junctional and extrajunctional regions of WT mice. In contrast, in mSOD mice 25HC markedly increased ganglioside GM1 labeling and decreased NBD-cholesterol fluorescence in both junctional and extrajunctional membranes (Fig. 5A, B). These data suggest that 25HC can enhance membrane microdomain formation and reduce membrane fluidity in mSOD mice. In support of this assumption, 25HC increased ratio of red/green F2N12S fluorescence in junctional (more pronounced) and extrajunctional regions of mSOD mice but not WT mice (Fig. 5C). This indicates on 25HC-induced increment of plasma membrane ordering in mSOD mice. Thus, plasma membranes of mSOD mice are more susceptible to 25HC, which can favor membrane microdomain formation. In addition, 25HC decreased uptake of BODIPY-Cer in junctional region of mSOD mice (Fig. 5D). In WT mice, 25HC had no marked influence on the Cer fluorescence.

Thus, 25HC changes membrane properties related with lipid rafts (GM1 ganglioside adoption, ordering, and fluidity) and uptake of Cer in opposite direction compared to the alterations observed in the junctional membranes of mSOD mice *vs* WT mice. It is tempting to suggest that elevation of 25HC could suppress ALS-related early changes in the membrane properties of NMJs.

Remarkably, in contrast to mSOD animals 25HC had a negligible influence on the membrane properties in WT mice. To test possibility that 25HC may be bound more effectively by membranes of mSOD mice, we used 25-(C4 TopFluor®) 25-OH cholesterol which is translocated by oxysterol-binding proteins [51,52] responsible for intracellular traffic of endogenous 25HC and Chol (Fig. 6). Uptake of 25-(C4 TopFluor®) 25-OH cholesterol was significantly higher in junctional regions of mSOD *vs* WT mice (Fig. 6A, B). Furthermore, pretreatment with 25HC markedly attenuated the 25-(C4 TopFluor®) 25-OH cholesterol uptake (Fig. 6B, C), suggesting a competition between these two sterols and, hence, the same mechanism responsible for their accumulation in the NMJs.

3.6. Effects of chronic treatment with oxysterol in mSOD mice

To assess effects of one-month treatment with very low dose of 25HC (0.4 mg/kg; one intraperitoneal injection per 4 days) F2N12S and fluorescent Cer were used. Similar to acute 25HC application, one-month treatment led to an increase in ratio of red/green F2N12S fluorescence in junctional regions of the SOD mice (Fig. 7A). In result, the ratio of the fluorescence in the junctional regions were similar in 25HC-treated mSOD and WT mice (1.26 ± 0.08, $n = 7$ *vs* 1.15 ± 0.07, $n = 8$). Uptake of fluorescent Cer into NMJs was decreased by the treatment (Fig. 7B). Eventually, Cer fluorescence in muscles of 25HC-treated mSOD mice was the same as than in WT mice (83.9 ± 4.7, $n = 9$ *vs*

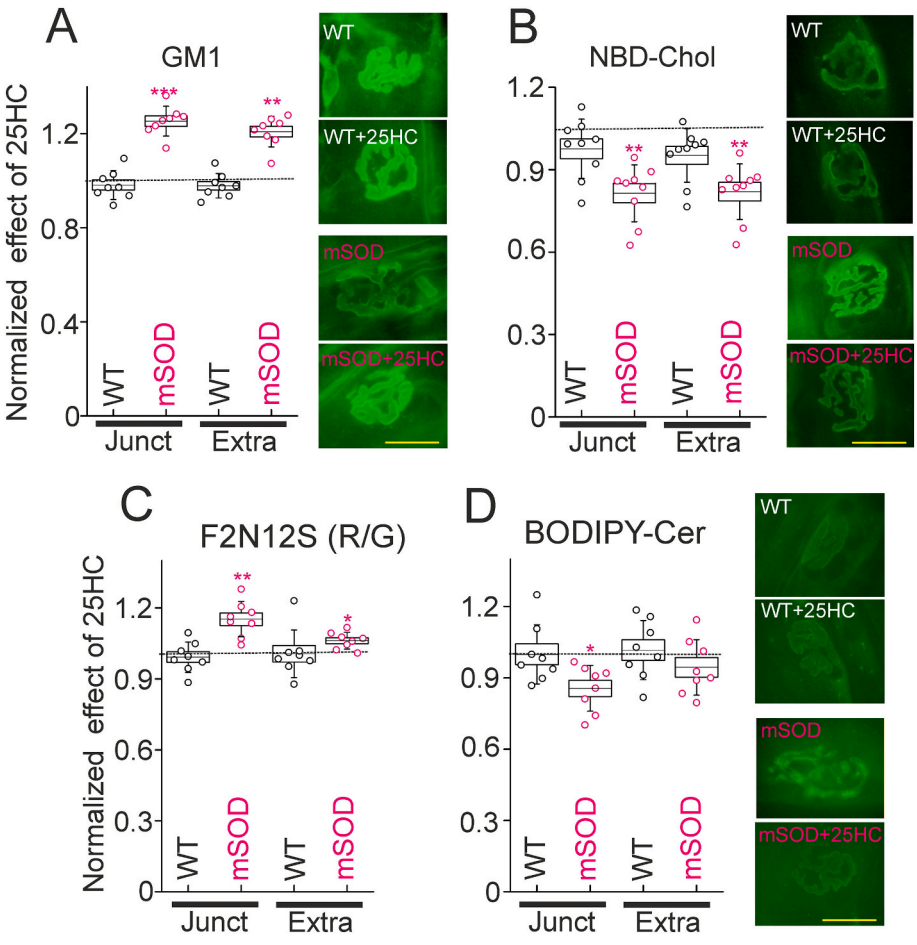

Fig. 5. Influence of acute exposure to 25HC on membrane properties in junctional and extrajunctional regions. Shown normalized effect on fluorescence of BODIPY-GM1 ganglioside (A), NBD-cholesterol (B), F2N12S dye (C), BODIPY-Cer (D). Y-axis represents the normalized effect of the oxysterol (1.0 is mean value of fluorescence intensity (A, B and D) or ratio of red/green fluorescence (C) in WT or mSOD samples without treatment with 25HC). A, C, D - N = 8 mice for each group (A/C/D: 216/177/202 and 224/185/211 muscle fibers for WT and mSOD, respectively). B - N = 9 per group (249 and 253 muscle fibers for WT and mSOD, respectively). Data are represented as mean ± SD; *$P < 0.05$, **$P < 0.01$, ***$P < 0.001$. (For interpretation of the references to colour in this figure legend, the reader is referred to the web version of this article.)

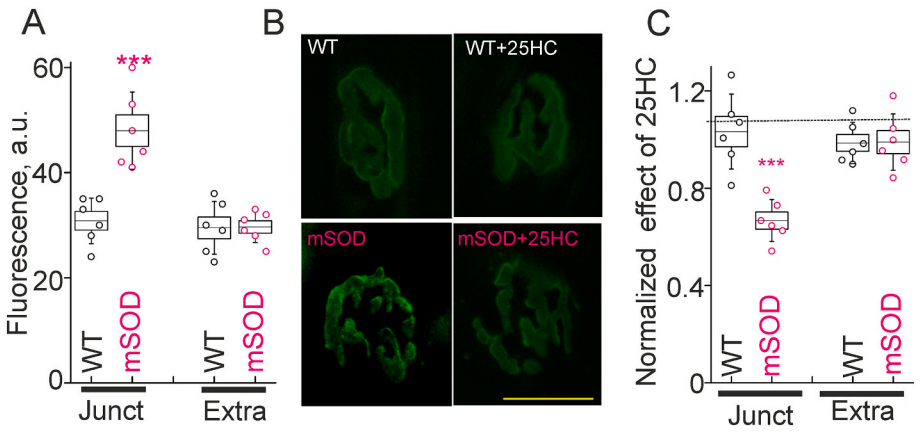

Fig. 6. Uptake of 25-(C4 TopFluor®) 25-OH cholesterol and influence of 25HC. A – Quantification of 25-(C4 TopFluor®) 25-OH cholesterol fluorescence. *N* = 6 per group (172 and 178 muscle fibers for WT and mSOD, respectively). B - Typical fluorescent image of junctional region in control and 25HC-pretreated muscles from WT and mSOD mice. Scale bar – 20 μm. C – Effect of 25HC on 25-(C4 TopFluor®) 25-OH cholesterol uptake. Y-axis represents the normalized effect of 25HC (1.0 – is mean value of fluorescence intensity in WT and mSOD muscles non-treated with 25HC). N = 6 for each group (167 and 173 muscle fibers for WT and mSOD, respectively); ***P ˂ 0.001.

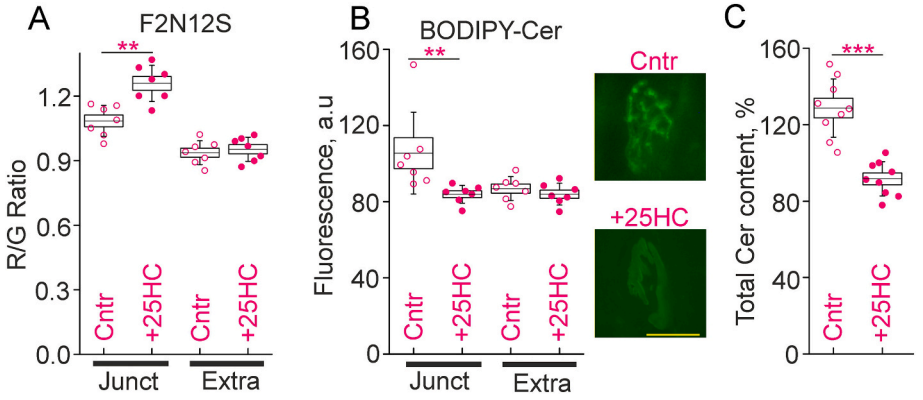

Fig. 7. Influence of chronical treatment with 25HC on lipid properties. Shown data obtained from 25HC-treated and control mSOD mice. A and B - Ratio of red / green F2N12S fluorescence and fluorescence of BODIPY-Cer in junctional and extrajunctional regions. C – Total amount of Cer in muscle homogenates. A, B - n = 7 mice per group (A/B: 149/187 and 152/193 muscle fibers for Cntr and + 25HC, respectively). C, *n* = 9 mice per group. Data are represented as mean ± SD; ** P˂0.01, ***P ˂ 0.001. (For interpretation of the references to colour in this figure legend, the reader is referred to the web version of this article.)

84.1 ± 6.7 n = 8). These data suggest that the chronic treatment with 25HC acts in the similar manner as acute 25HC application and can prevent the early membrane disturbances in mSOD mice. Furthermore, administration of 25HC decreased total content of Cer in muscle of mSOD mice, bringing it to close to WT value (Fig. 7C). This points to a persistent effect of the treatment.

In addition, acute application of 25HC lost the effects on ratio of red/green F2N12S fluorescence as well as on Cer uptake in muscle from the mSOD mice chronically treated with 25HC (Suppl. Fig. 2). This implies that acute and long-term administration of 25HC may act on similar targets in mSOD mice.

To estimate influence of the long-term treatment with 25HC on NMJs, we analyzed morphology, ACh levels and lipid peroxidation (Fig. 8). Increase in number of end plate islets (fragmentation) occurs with aging and has also been observed early in mouse models of muscular dystrophy [66,67] as well as in SOD-G37R mice [68]. Furthermore, fragmentation can be induced by crush- or laser-induced muscle fiber damage [69,70]. In ALS patients, fragmentation of postsynaptic apparatus is present at early disease stage [8]. In symptomatic SOD-G93A mice, fragmentation of end plate together with decrease in density of postsynaptic ACh receptors were observed in the extensor digitorum longus [71], but not in soleus muscle [7]. Currently, fragmentation can be considered as a form regeneration [72]. The morphometric analysis of nAChR distribution showed an increase in the number of end plate islets in diaphragm of mSOD mice (Fig. 8A). The one-month treatment with 25HC prevented the fragmentation of NMJs in mSOD mice. The mean areas of NMJs were similar in all groups (Suppl. Fig. 3). Importantly, the chronic administration of 25HC suppressed an increase in extracellular levels of choline in muscle of mSOD mice (Fig. 8B), suggesting a mitigation of dysregulation in non-quantum

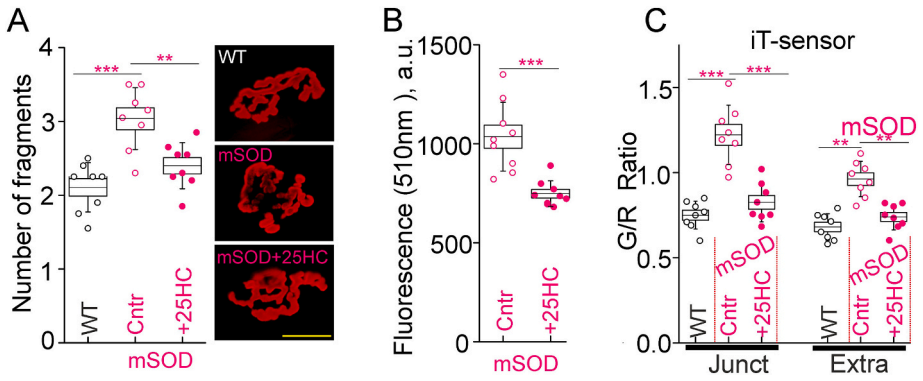

Fig. 8. Effect of chronical administration of 25HC on indications of neuromuscular abnormality in mSOD mice. A – Analysis of NMJ fragmentation (left) and typical images of αBtx-labeled NMJs (right) in WT and mSOD (control and treated with 25HC) mice. B – Differences in extracellular choline/ACh levels. C - Lipid peroxidation. Shown ratio of green / red fluorescence of iT sensor, an indicator of membrane lipid peroxidation. A, C - N = 8 mice for each group (A/C: 225/164, 233/171 and 236/174 muscle fibers for WT, Cntr and + 25HC, respectively). D - N = 8 mice per group. Data are represented as mean ± SD; **P˂0.01, ***P ˂ 0.001. (For interpretation of the references to colour in this figure legend, the reader is referred to the web version of this article.)

neurotransmitter release.

Oxidative damage of membrane lipids is early sign of ALS as well as NMJ dysfunction [73,74]. Assessment with iT-indicator pointed to an enhancement of lipid peroxidation in the junctional region of mSOD mice at pre-onset stage (Fig. 8C). Along the same lines, hydroperoxide levels in the muscle (but not spinal cord) were twice higher in mSOD *vs* WT mice (Suppl. Fig. 4). The long-term treatment with 25HC prevented the increase in ratio of green/red iT-sensor fluorescence in the synaptic regions indicating on preclusion of oxidative lipid modifications. Thus, chronic administration of 25HC seems to mitigate the early abnormalities in diaphragm muscle of mSOD mice.

4. Discussion

The main findings of the present study are: lipid membrane differences in junctional compartment occur early in pre-onset stage of the ALS model mice; this is accompanied by increase in extracellular choline levels and NMJ fragmentation; chronic treatment with 25HC can prevent the changes in membrane lipids, choline levels and NMJs morphology. In contrast to the mutant mice, NMJs of WT mice were not sensitive to 25HC likely due to lower ability to bind the oxysterol. The latter additionally points to marked alterations in lipid homeostasis in mSOD mice.

The early lipid abnormalities in mSOD mice represented a decrease in labeling with lipid raft markers, increase in membrane fluidity and disordering. All these changes indicate on a disturbance of lipid raft integrity in mSOD mice. Given that the alterations were more pronounced in junctional regions compared to extrajunctional sites, the NMJ membranes seem to be a more vulnerable to the disease-related lipid disbalance. Consistent with these findings, marked changes in abundance (mainly downregulation) of proteins in the raft fraction were demonstrated in spinal cord of the onset stage SOD(G93A) mice. Among these altered proteins, about 20% were involved in presynaptic vesicular traffic and neurotransmitter release [75]. A loss of function of Sigma receptors, observed in sporadic ALS, caused a destabilization of lipid rafts in motor neuron-like NSC34 cells, thereby leading to impaired $[Ca^{2+}]_{in}$ mobilization and endosomal trafficking [76].

Decrease in lipid raft integrity can be mediated by depletion of Chol, that serves as a "glue" for raft formation. However, levels of Chol in muscle homogenates were unaffected in mSOD mice. Likewise, Chol content in primary cortical neurons from SOD(G93A) mice was similar to that in WT mice [77]. Cer accumulation can reduce lipid raft stability in disused muscles prior to onset of atrophy [45,47,50]. Herein, we found significantly higher Cer levels in pre-onset stage mSOD mice that was accompanied by enhanced ability to accumulate exogenous Cer selectively in NMJs. Importantly, excess Cer was detected in spinal cord of ALS patients [20]. Buildup of Cer in spinal cord appeared in SOD1 (G93A) and SOD1(G86R) mice prior to manifestation of ALS signs [20,78]. These data point to Cer deposition and lipid raft disturbance in NMJs as potentially interconnected events in the pre-onset stage of the pathology.

Studies using Chol extraction or oxidation as approaches for raft disturbance suggest that neuromuscular transmission is a quite sensitive to reduction of lipid raft integrity [23]. In NMJs, slight Chol depletion markedly increased extracellular choline/ACh levels (due to enhanced non-quantum release) [42] and suppressed a recovery of evoked neurotransmitter release after episode of 20 Hz stimulation [79]. Similarly, lipid raft-destabilizing oxysterol, 5α-cholestan-3-one, depressed a recovery of evoked ACh release after 20-Hz stimulus train in NMJs [26,46]. Also, moderate Chol depletion facilitated spontaneous ACh exocytosis in NMJs [56,80,81]. Accordingly, the observed at pre-onset stage changes in ACh releases (specifically, marked increase in extracellular choline levels, enhancement of spontaneous exocytosis and suppression of evoked release recovery after 20 Hz stimulation) can be caused by a loss of lipid raft integrity. Supporting this assumption is that Chol supplementation of plasma membranes (a raft-stabilizing manipulation) reduced the extracellular choline content in mSOD mice. This may reflect suppression of non-quantum ACh release. Note that excess ACh can aggravate degeneration of NMJs in mSOD mice and cause prematurely age-related structural alterations (including fragmentation) of NMJs [82].

In mSOD mice, we found changes in MEPCs (increase in amplitudes but decrease in rise and decay times) which can arise from early postsynaptic abnormalities. This result ties well with previous study wherein increase in amplitude and decrease in rise time of miniature end plate potentials were detected in diaphragm of the pre-onset stage SOD1 (G93A) mice [13]. These abnormalities could be linked with alteration in nAChR clusterization, namely fragmentation of end plates in the mSOD mice. It should be noted that lipid rafts participate in control of nAChR distribution and activity [23,83]. Hence, the lipid raft disintegration might contribute to fragmentation of nAChR clusters and changes in their functionality. Chol addition can stabilize nAChR cluster, rescuing junctional regions from fragmentation in the denervated muscle [84].

Decrease in decay time of MEPCs can reflect alteration in AChE activity in mSOD mice. In one study, downregulation of AChE was found in muscle biopsies from ALS patients [85]. Fraction of AChE can be anchored in synaptic membranes due to interaction with lipid rafts [86]. However, decay time of EPCs was the similar in mSOD and WT mice. Furthermore, addition of exogenous AChE did not modify the percentage of increase in choline levels in mSOD mice compared to WT animals. These facts suggest no marked difference in activity of native AChE in mSOD *vs* WT mice.

Lipid raft disturbance can induce oxidative stress *via* different mechanisms [56,87]. Particularly, Chol depletion caused a rise of NADPH oxidase-dependent ROS production as well as lipid peroxidation in NMJs [56]. Herein, we found increased levels of hydroperoxides in muscle homogenates and signs of lipid peroxidation in NMJs of mSOD mice. Hypothetically, these can represent consequences of the lipid raft disorganization. Notably, lipid hydroperoxides can modify SOD1 protein, promoting its aggregation, which may have detrimental effects [88].

Oxidized Chol derivatives are important class of modulators for numerous cellular functions, including neuromuscular transmission [23,89]. Pronounced changes in levels of some oxysterols during neurodegenerative diseases allow to consider the oxysterols as markers of the disorders and (or) contributors to their pathogenesis [90,91]. Among oxysterols, levels of 25HC in serum and CSF were higher in ALS patients with about one-year duration of the disease *vs* healthy controls. Furthermore, mRNA expression of 25HC-producing enzymes was enhanced in brain of mSOD1(G93A) mice at the pre-onset stage, but decreased later [30]. Levels of 7α,25-dihydroxycholest-4-en-3-one, a derivative of 25HC, were also higher in serum, but lower in CSF of ALS patients [31]. Accordingly, 25HC can be implicated in ALS. Production of 25HC is drastically upregulated by numerous inflammatory stimuli [36,37,92]. In turn, the increase in 25HC can regulate multiple aspects of the immune response, thereby forming negative and positive feedback loops [92]. Overall, 25HC exerts antiviral and cardioprotective activities as well as modulates inflammation and Chol metabolism [37,92–94]. Herein, we found that acute application of 25HC increased lipid ordering and insertion of ganglioside GM1 in the plasma membrane as well as decreased membrane fluidity and Cer uptake in NMJs of mSOD mice. Hence, 25HC favors lipid raft formation and can suppress Cer accumulation in NMJs of mSOD mice. These results are in agreement with previous studies showing the ability of 25HC: to promote microdomains formation in model membranes from mixtures of the saturated and unsaturated lipids [95] and to alter Cer traffic *via* membrane contact sites [96,97]. Furthermore, 25HC may affect cellular Chol redistribution *via* changing Chol transport through membrane contact sites [94].

Importantly, that 25HC affected the membranes only in mSOD mice, whereas it had no marked influence in WT mice. Alterations in functionality of binding sites for 25HC (*e.g.*, numerous oxysterol-binding

proteins) can be responsible for a higher sensitivity of the membranes from mSOD mice to 25HC. Two observations imply an engagement of oxysterol-binding proteins in ALS. First, an important regulator of oxysterol-binding protein function vesicle-associated membrane protein-associated protein B (VAPB) is downregulated in spinal cord of ALS patients and mSOD mice at onset stage [98]. Second, mutations in VAPB cause a familial form of ALS and overexpression of oxysterol-binding proteins can reduce the mutant VAPB phenotype in HeLa cells [99,100]. Note that oxysterol-binding proteins can mediate effects of 25HC on Cer traffic and membrane Chol distribution [94,96,97]. Herein, we found that fluorescent 25-(C4 TopFluor®) 25-OH cholesterol that selectively interacts with oxysterol-binding proteins [51,52] was uptaken more effectively into NMJs of mSOD mice and 25HC can compete with the uptake of 25-(C4 TopFluor®) 25-OH cholesterol. Accordingly, a higher ability to trap the oxysterol may be reason why 25HC preferentially affected the lipid properties in mSOD mice. Importantly, 25HC altered the lipid properties in opposite direction compared to the changes observed in NMJs of mSOD *vs* WT mice. This suggests a possibility that long-term administration of 25HC can affect NMJs in the ALS model mice. Indeed, chronical treatment with 25HC prevented the decrease in lipid ordering as well as upregulation of both Cer levels and fluorescent Cer uptake into NMJs of mSOD mice. Additionally, the long-term application of 25HC precluded the appearance of synaptic abnormalities, namely lipid peroxidation, increased extracellular choline levels and nAChR cluster fragmentation.

Thus, 25HC could counteract early ALS-related changes in NMJs and, hence, elevation of 25HC in ALS patients might represent a compensatory mechanism. In case of ALS, there is a unique situation when hypercholesterinemia has beneficial effects whereas Chol-decreasing drugs aggravate the pathology [20–24]. The levels of 25HC are elevated in hypercholesterolemic serum and decreased in response to statin treatment [64,65]. Speculatively, an increase in 25HC levels could be responsible for positive effect of hypercholesterinemia in ALS.

5. Conclusion

In sum, the present study highlighted on early alterations in membrane properties, including lipid raft disturbance and increase in Cer accumulation, at NMJs in the diaphragm muscle of mSOD mice. Simultaneously, indications of synaptic abnormalities, including lipid peroxidation, increase in extracellular choline and fragmentation of nAChR clusters, appear. Immune-related oxysterol 25HC alleviates these alterations in the membrane and synaptic properties. We suggest that membrane abnormalities in NMJs can occur very early in ALS and be connected with synaptic changes. Limitations of this study are using mainly fluorescent approaches and one type of muscle. Accordingly, further genetic and molecular studies as well as using other muscle types are required to reveal the precise molecular mechanism(s) by which membrane properties, Cer and 25HC are involved in ALS.

Supplementary data to this article can be found online at https://doi.org/10.1016/j.lfs.2021.119300.

Funding

This study was supported in part by the Russian Foundation for Basic Research grant #20–04-00077 (3.5–3.6), Russian Science Foundation grant #19–15-00329 (3.1–3.4) and partially the government assignment for FRC Kazan Scientific Center of RAS (for AMP).

CRediT authorship contribution statement

Guzel F. Zakyrjanova: Investigation, Formal analysis, Visualization. **Arthur R. Giniatullin:** Investigation, Formal analysis, Visualization. **Kamilla A. Mukhutdinova:** Investigation, Formal analysis, Visualization. **Eva A. Kuznetsova:** Investigation. **Alexey M. Petrov:** Conceptualization, Supervision, Writing – review & editing, Funding acquisition.

Declaration of competing interest

The authors declare that they have no known competing financial interests or personal relationships that could have appeared to influence the work reported in this paper.

Acknowledgements

We thank Dr. A.V. Zakharov (Kazan Federal University) for technical assistance. Author contributions: G. Z., A.G., K.M., E.K. produced and analyzed data. A.G. and A.P. interpreted results of experiments. A.P. designed the research and wrote the manuscript. All the authors approved the final version of the manuscript.

References

[1] J. Nijssen, L.H. Comley, E. Hedlund, Motor neuron vulnerability and resistance in amyotrophic lateral sclerosis, Acta Neuropathol. 133 (6) (2017) 863–885, https://doi.org/10.1007/s00401-017-1708-8.
[2] L.R. Fischer, D.G. Culver, P. Tennant, A.A. Davis, M. Wang, A. Castellano-Sanchez, et al., Amyotrophic lateral sclerosis is a distal axonopathy: evidence in mice and man, Exp. Neurol. 185 (2) (2004) 232–240, https://doi.org/10.1016/j.expneurol.2003.10.004.
[3] Liu KX, Edwards B, Lee S, Finelli MJ, Davies B, Davies KE, et al. Neuron-specific antioxidant OXR1 extends survival of a mouse model of amyotrophic lateral sclerosis. Brain. 2015;138(Pt 5):1167–81. doi: https://doi.org/10.1093/brain/awv039.
[4] S. Vinsant, C. Mansfield, R. Jimenez-Moreno, V. Del Gaizo Moore, M. Yoshikawa, T.G. Hampton, et al., Characterization of early pathogenesis in the SOD1(G93A) mouse model of ALS: part II, results and discussion, Brain Behav 3 (4) (2013) 431–457, https://doi.org/10.1002/brb3.142.
[5] D. Frey, C. Schneider, L. Xu, J. Borg, W. Spooren, P. Caroni, Early and selective loss of neuromuscular synapse subtypes with low sprouting competence in motoneuron diseases, J. Neurosci. 20 (7) (2000) 2534–2542.
[6] T.W. Gould, R.R. Buss, S. Vinsant, D. Prevette, W. Sun, C.M. Knudson, et al., Complete dissociation of motor neuron death from motor dysfunction by Bax deletion in a mouse model of ALS, J. Neurosci. 26 (34) (2006) 8774–8786, https://doi.org/10.1523/JNEUROSCI.2315-06.2006.
[7] H. Narai, Y. Manabe, M. Nagai, I. Nagano, Y. Ohta, T. Murakami, et al., Early detachment of neuromuscular junction proteins in ALS mice with SODG93A mutation, Neurol. Int. 1 (1) (2009), e16, https://doi.org/10.4081/ni.2009.e16.
[8] G. Bruneteau, S. Bauche, J.L. Gonzalez de Aguilar, G. Brochier, N. Mandjee, M. L. Tanguy, et al., Endplate denervation correlates with Nogo-a muscle expression in amyotrophic lateral sclerosis patients, Ann Clin Transl Neurol 2 (4) (2015) 362–372, https://doi.org/10.1002/acn3.179.
[9] M. Dewil, V.F. dela Cruz, L. Van Den Bosch, W. Robberecht, Inhibition of p38 mitogen activated protein kinase activation and mutant SOD1(G93A)-induced motor neuron death, Neurobiol. Dis. 26 (2) (2007) 332–341, https://doi.org/10.1016/j.nbd.2006.12.023.
[10] C. Rouaux, I. Panteleeva, F. Rene, J.L. Gonzalez de Aguilar, A. Echaniz-Laguna, L. Dupuis, et al., Sodium valproate exerts neuroprotective effects in vivo through CREB-binding protein-dependent mechanisms but does not improve survival in an amyotrophic lateral sclerosis mouse model, J. Neurosci. 27 (21) (2007) 5535–5545, https://doi.org/10.1523/JNEUROSCI.1139-07.2007.
[11] G. Dobrowolny, M. Aucello, E. Rizzuto, S. Beccafico, C. Mammucari, S. Boncompagni, et al., Skeletal muscle is a primary target of SOD1G93A-mediated toxicity, Cell Metab. 8 (5) (2008) 425–436, https://doi.org/10.1016/j.cmet.2008.09.002.
[12] M. Wong, L.J. Martin, Skeletal muscle-restricted expression of human SOD1 causes motor neuron degeneration in transgenic mice, Hum. Mol. Genet. 19 (11) (2010) 2284–2302, https://doi.org/10.1093/hmg/ddq106.
[13] M.C. Rocha, P.A. Pousinha, A.M. Correia, A.M. Sebastiao, J.A. Ribeiro, Early changes of neuromuscular transmission in the SOD1(G93A) mice model of ALS start long before motor symptoms onset, PLoS One 8 (9) (2013), e73846, https://doi.org/10.1371/journal.pone.0073846.
[14] F. Nascimento, A.M. Sebastiao, J.A. Ribeiro, Presymptomatic and symptomatic ALS SOD1(G93A) mice differ in adenosine A1 and A2A receptor-mediated tonic modulation of neuromuscular transmission, Purinergic Signal 11 (4) (2015) 471–480, https://doi.org/10.1007/s11302-015-9465-4.
[15] D. Arbour, E. Tremblay, E. Martineau, J.P. Julien, R. Robitaille, Early and persistent abnormal decoding by glial cells at the neuromuscular junction in an ALS model, J. Neurosci. 35 (2) (2015) 688–706, https://doi.org/10.1523/JNEUROSCI.1379-14.2015.
[16] L. Just-Borras, E. Hurtado, V. Cilleros-Mane, O. Biondi, F. Charbonnier, M. Tomas, et al., Overview of impaired BDNF signaling, their coupled downstream serine-threonine kinases and SNARE/SM complex in the neuromuscular junction of the amyotrophic lateral sclerosis model SOD1-G93A mice, Mol. Neurobiol. 56 (10) (2019) 6856–6872, https://doi.org/10.1007/s12035-019-1550-1.

[17] R. Maimon, A. Ionescu, A. Bonnie, S. Sweetat, S. Wald-Altman, S. Inbar, et al., miR126-5p downregulation facilitates axon degeneration and NMJ disruption via a non-cell-autonomous mechanism in ALS, J. Neurosci. 38 (24) (2018) 5478–5494, https://doi.org/10.1523/JNEUROSCI.3037-17.2018.
[18] L. Duplan, N. Bernard, W. Casseron, K. Dudley, E. Thouvenot, J. Honnorat, et al., Collapsin response mediator protein 4a (CRMP4a) is upregulated in motoneurons of mutant SOD1 mice and can trigger motoneuron axonal degeneration and cell death, J. Neurosci. 30 (2) (2010) 785–796, https://doi.org/10.1523/JNEUROSCI.5411-09.2010.
[19] S.M. Kim, H. Kim, J.E. Kim, K.S. Park, J.J. Sung, S.H. Kim, et al., Amyotrophic lateral sclerosis is associated with hypolipidemia at the presymptomatic stage in mice, PLoS One 6 (3) (2011), e17985, https://doi.org/10.1371/journal.pone.0017985.
[20] R.G. Cutler, W.A. Pedersen, S. Camandola, J.D. Rothstein, M.P. Mattson, Evidence that accumulation of ceramides and cholesterol esters mediates oxidative stress-induced death of motor neurons in amyotrophic lateral sclerosis, Ann. Neurol. 52 (4) (2002) 448–457, https://doi.org/10.1002/ana.10312.
[21] L. Dupuis, P. Corcia, A. Fergani, J.L. Gonzalez De Aguilar, D. Bonnefont-Rousselot, R. Bittar, et al., Dyslipidemia is a protective factor in amyotrophic lateral sclerosis, Neurology 70 (13) (2008) 1004–1009, https://doi.org/10.1212/01.wnl.0000285080.70324.27.
[22] Z. Zheng, L. Sheng, H. Shang, Statins and amyotrophic lateral sclerosis: a systematic review and meta-analysis, Amyotroph Lateral Scler Frontotemporal Degener 14 (4) (2013) 241–245, https://doi.org/10.3109/21678421.2012.732078.
[23] I.I. Krivoi, A.M. Petrov, Cholesterol and the safety factor for neuromuscular transmission, Int. J. Mol. Sci. 20 (5) (2019), https://doi.org/10.3390/ijms20051046.
[24] C. Ingre, L. Chen, Y. Zhan, J. Termorshuizen, L. Yin, F. Fang, Lipids, apolipoproteins, and prognosis of amyotrophic lateral sclerosis, Neurology 94 (17) (2020), e1835-e44, https://doi.org/10.1212/WNL.0000000000009322.
[25] J.J. Weber, L.E. Clemensson, H.B. Schioth, H.P. Nguyen, Olesoxime in neurodegenerative diseases: Scrutinising a promising drug candidate, Biochem. Pharmacol. 168 (2019) 305–318, https://doi.org/10.1016/j.bcp.2019.07.002.
[26] M.R. Kasimov, G.F. Zakyrjanova, A.R. Giniatullin, A.L. Zefirov, A.M. Petrov, Similar oxysterols may lead to opposite effects on synaptic transmission: Olesoxime versus 5alpha-cholestan-3-one at the frog neuromuscular junction, Biochim. Biophys. Acta 1861 (7) (2016) 606–616, https://doi.org/10.1016/j.bbalip.2016.04.010.
[27] G.F. Zakyrjanova, A.I. Gilmutdinov, A.N. Tsentsevitsky, A.M. Petrov, Olesoxime, a cholesterol-like neuroprotectant restrains synaptic vesicle exocytosis in the mice motor nerve terminals: possible role of VDACs, Biochim. Biophys. Acta Mol. Cell Biol. Lipids (2020), 158739, https://doi.org/10.1016/j.bbalip.2020.158739.
[28] A. Sawada, S. Wang, M. Jian, J. Leem, J. Wackerbarth, J. Egawa, et al., Neuron-targeted caveolin-1 improves neuromuscular function and extends survival in SOD1(G93A) mice, FASEB J. 33 (6) (2019) 7545–7554, https://doi.org/10.1096/fj.201802652RR.
[29] J. Mojsilovic-Petrovic, G.B. Jeong, A. Crocker, A. Arneja, S. David, D.S. Russell, et al., Protecting motor neurons from toxic insult by antagonism of adenosine A2a and Trk receptors, J. Neurosci. 26 (36) (2006) 9250–9263, https://doi.org/10.1523/JNEUROSCI.1856-06.2006.
[30] S.M. Kim, M.Y. Noh, H. Kim, S.Y. Cheon, K.M. Lee, J. Lee, et al., 25-hydroxycholesterol is involved in the pathogenesis of amyotrophic lateral sclerosis, Oncotarget 8 (7) (2017) 11855–11867, https://doi.org/10.18632/oncotarget.14416.
[31] J. Abdel-Khalik, E. Yutuc, P.J. Crick, J.A. Gustafsson, M. Warner, G. Roman, et al., Defective cholesterol metabolism in amyotrophic lateral sclerosis, J. Lipid Res. 58 (1) (2017) 267–278, https://doi.org/10.1194/jlr.P071639.
[32] S.R. Pfohl, M.T. Halicek, C.S. Mitchell, Characterization of the contribution of genetic background and gender to disease progression in the SOD1 G93A mouse model of amyotrophic lateral sclerosis: a meta-analysis, J Neuromuscul Dis 2 (2) (2015) 137–150, https://doi.org/10.3233/JND-140068.
[33] M.E. Gurney, H. Pu, A.Y. Chiu, M.C. Dal Canto, C.Y. Polchow, D.D. Alexander, et al., Motor neuron degeneration in mice that express a human Cu,Zn superoxide dismutase mutation, Science 264 (5166) (1994) 1772–1775, https://doi.org/10.1126/science.8209258.
[34] M.R. Kasimov, M.R. Fatkhrakhmanova, K.A. Mukhutdinova, A.M. Petrov, 24S-hydroxycholesterol enhances synaptic vesicle cycling in the mouse neuromuscular junction: implication of glutamate NMDA receptors and nitric oxide, Neuropharmacology 117 (2017) 61–73, https://doi.org/10.1016/j.neuropharm.2017.01.030.
[35] K.A. Mukhutdinova, M.R. Kasimov, G.F. Zakyrjanova, M.R. Gumerova, A. M. Petrov, Oxysterol modulates neurotransmission via liver-X receptor/NO synthase-dependent pathway at the mouse neuromuscular junctions, Neuropharmacology 150 (2019) 70–79, https://doi.org/10.1016/j.neuropharm.2019.03.018.
[36] C. Shen, J. Zhou, X. Wang, X.Y. Yu, C. Liang, B. Liu, et al., Angiotensin-II-induced muscle wasting is mediated by 25-hydroxycholesterol via GSK3beta signaling pathway, EBioMedicine 16 (2017) 238–250, https://doi.org/10.1016/j.ebiom.2017.01.040.
[37] D.R. Bauman, A.D. Bitmansour, J.G. McDonald, B.M. Thompson, G. Liang, D. W. Russell, 25-Hydroxycholesterol secreted by macrophages in response to toll-like receptor activation suppresses immunoglobulin A production, Proc. Natl. Acad. Sci. U. S. A. 106 (39) (2009) 16764–16769, https://doi.org/10.1073/pnas.0909142106.
[38] K.A. Mukhutdinova, M.R. Kasimov, A.R. Giniatullin, G.F. Zakyrjanova, A. M. Petrov, 24S-hydroxycholesterol suppresses neuromuscular transmission in SOD1(G93A) mice: a possible role of NO and lipid rafts, Mol. Cell. Neurosci. 88 (2018) 308–318, https://doi.org/10.1016/j.mcn.2018.03.006.
[39] A. Giniatullin, A. Petrov, R. Giniatullin, Action of hydrogen peroxide on synaptic transmission at the mouse neuromuscular junction, Neuroscience 399 (2019) 135–145, https://doi.org/10.1016/j.neuroscience.2018.12.027.
[40] M.I. Glavinovic, Voltage clamping of unparalysed cut rat diaphragm for study of transmitter release, J. Physiol. 290 (2) (1979) 467–480, https://doi.org/10.1113/jphysiol.1979.sp012784.
[41] A.V. Zakharov, Elph: an open-source program for acquisition control and analysis of electrophysiological signals, Uchenye Zapiski Kazanskogo Universiteta Seriya Estestvennye Nauki 161 (2) (2019) 245–254, https://doi.org/10.26907/2542-064x.2019.2.245-254.
[42] A.M. Petrov, N.V. Naumenko, K.V. Uzinskaya, A.R. Giniatullin, A.K. Urazaev, A. L. Zefirov, Increased non-quantal release of acetylcholine after inhibition of endocytosis by methyl-beta-cyclodextrin: the role of vesicular acetylcholine transporter, Neuroscience 186 (2011) 1–12, https://doi.org/10.1016/j.neuroscience.2011.04.051.
[43] V.V. Kravtsova, A.M. Petrov, V.V. Matchkov, E.V. Bouzinova, A.N. Vasiliev, B. Benziane, et al., Distinct alpha2 Na,K-ATPase membrane pools are differently involved in early skeletal muscle remodeling during disuse, J Gen Physiol 147 (2) (2016) 175–188, https://doi.org/10.1085/jgp.201511494.
[44] V.V. Kravtsova, A.M. Petrov, A.N. Vasil'ev, A.L. Zefirov, I.I. Krivoi, Role of cholesterol in the maintenance of endplate electrogenesis in rat diaphragm, Bull. Exp. Biol. Med. 158 (3) (2015) 298–300, https://doi.org/10.1007/s10517-015-2745-8.
[45] Petrov AM, Kravtsova VV, Matchkov VV, Vasiliev AN, Zefirov AL, Chibalin AV, et al. Membrane lipid rafts are disturbed in the response of rat skeletal muscle to short-term disuse. Am. J. Phys. Cell Phys. 2017;312(5):C627-C37. doi: https://doi.org/10.1152/ajpcell.00365.2016.
[46] M.R. Kasimov, A.R. Giniatullin, A.L. Zefirov, A.M. Petrov, Effects of 5alpha-cholestan-3-one on the synaptic vesicle cycle at the mouse neuromuscular junction, Biochim. Biophys. Acta 1851 (5) (2015) 674–685, https://doi.org/10.1016/j.bbalip.2015.02.012.
[47] I.G. Bryndina, M.N. Shalagina, A.V. Sekunov, A.L. Zefirov, A.M. Petrov, Clomipramine counteracts lipid raft disturbance due to short-term muscle disuse, Neurosci. Lett. 664 (2018) 1–6, https://doi.org/10.1016/j.neulet.2017.11.009.
[48] U.G. Odnoshivkina, V.I. Sytchev, L.F. Nurullin, A.R. Giniatullin, A.L. Zefirov, A. M. Petrov, β2-adrenoceptor agonist-evoked reactive oxygen species generation in mouse atria: implication in delayed inotropic effect, Eur. J. Pharmacol. 765 (2015) 140–153, https://doi.org/10.1016/j.ejphar.2015.08.020.
[49] S. Oncul, A.S. Klymchenko, O.A. Kucherak, A.P. Demchenko, S. Martin, M. Dontenwill, et al., Liquid ordered phase in cell membranes evidenced by a hydration-sensitive probe: effects of cholesterol depletion and apoptosis, Biochim. Biophys. Acta 1798 (7) (2010) 1436–1443, https://doi.org/10.1016/j.bbamem.2010.01.013.
[50] A.M. Petrov, M.N. Shalagina, V.A. Protopopov, V.G. Sergeev, S.V. Ovechkin, N. G. Ovchinina, et al., Changes in membrane ceramide pools in rat soleus muscle in response to short-term disuse, Int. J. Mol. Sci. 20 (19) (2019), https://doi.org/10.3390/ijms20194860.
[51] M. Holtta-Vuori, R.L. Uronen, J. Repakova, E. Salonen, I. Vattulainen, P. Panula, et al., BODIPY-cholesterol: a new tool to visualize sterol trafficking in living cells and organisms, Traffic 9 (11) (2008) 1839–1849, https://doi.org/10.1111/j.1600-0854.2008.00801.x.
[52] M. Jansen, Y. Ohsaki, L.R. Rega, R. Bittman, V.M. Olkkonen, E. Ikonen, Role of ORPs in sterol transport from plasma membrane to ER and lipid droplets in mammalian cells, Traffic 12 (2) (2011) 218–231, https://doi.org/10.1111/j.1600-0854.2010.01142.x.
[53] A.V. Zakharov, A.M. Petrov, N.V. Kotov, A.L. Zefirov, Experimental and modeling investigation of the mechanism of synaptic vesicles recycling, Biophysics 57 (4) (2012) 508–518, https://doi.org/10.1134/s0006350912040203.
[54] P. Fletcher, T. Forrester, The effect of curare on the release of acetylcholine from mammalian motor nerve terminals and an estimate of quantum content, J. Physiol. 251 (1) (1975) 131–144, https://doi.org/10.1113/jphysiol.1975.sp011084.
[55] F. Vyskocil, A.I. Malomouzh, E.E. Nikolsky, Non-quantal acetylcholine release at the neuromuscular junction, Physiol. Res. 58 (6) (2009) 763–784.
[56] A.M. Petrov, A.A. Yakovleva, A.L. Zefirov, Role of membrane cholesterol in spontaneous exocytosis at frog neuromuscular synapses: reactive oxygen species-calcium interplay, J. Physiol. 592 (22) (2014) 4995–5009, https://doi.org/10.1113/jphysiol.2014.279695.
[57] G. Margheri, R. D'Agostino, S. Trigari, S. Sottini, M. Del Rosso, The beta-subunit of cholera toxin has a high affinity for ganglioside GM1 embedded into solid supported lipid membranes with a lipid raft-like composition, Lipids 49 (2) (2014) 203–206, https://doi.org/10.1007/s11745-013-3845-8.
[58] Ichikawa N, Iwabuchi K, Kurihara H, Ishii K, Kobayashi T, Sasaki T, et al. Binding of laminin-1 to monosialoganglioside GM1 in lipid rafts is crucial for neurite outgrowth. J. Cell Sci.. 2009;122(Pt 2):289–99. doi: https://doi.org/10.1242/jcs.030338.
[59] P. Ostasov, J. Sykora, J. Brejchova, A. Olzynska, M. Hof, P. Svoboda, FLIM studies of 22- and 25-NBD-cholesterol in living HEK293 cells: plasma membrane change induced by cholesterol depletion, Chem. Phys. Lipids 167-168 (2013) 62–69, https://doi.org/10.1016/j.chemphyslip.2013.02.006.
[60] V. Kilin, O. Glushonkov, L. Herdly, A. Klymchenko, L. Richert, Y. Mely, Fluorescence lifetime imaging of membrane lipid order with a ratiometric

fluorescent probe, Biophys. J. 108 (10) (2015) 2521–2531, https://doi.org/10.1016/j.bpj.2015.04.003.
[61] V.V. Shynkar, A.S. Klymchenko, C. Kunzelmann, G. Duportail, C.D. Muller, A. P. Demchenko, et al., Fluorescent biomembrane probe for ratiometric detection of apoptosis, J. Am. Chem. Soc. 129 (7) (2007) 2187–2193, https://doi.org/10.1021/ja068008h.
[62] P.T. Reidy, Z.S. Mahmassani, A.I. McKenzie, J.J. Petrocelli, S.A. Summers, M. J. Drummond, Influence of exercise training on skeletal muscle insulin resistance in aging: spotlight on muscle ceramides, Int. J. Mol. Sci. 21 (4) (2020), https://doi.org/10.3390/ijms21041514.
[63] J. Rohrbough, E. Rushton, L. Palanker, E. Woodruff, H.J. Matthies, U. Acharya, et al., Ceramidase regulates synaptic vesicle exocytosis and trafficking, J. Neurosci. 24 (36) (2004) 7789–7803, https://doi.org/10.1523/JNEUROSCI.1146-04.2004.
[64] I.H.K. Dias, I. Milic, G.Y.H. Lip, A. Devitt, M.C. Polidori, H.R. Griffiths, Simvastatin reduces circulating oxysterol levels in men with hypercholesterolaemia, Redox Biol. 16 (2018) 139–145, https://doi.org/10.1016/j.redox.2018.02.014.
[65] K.A. Johnson, C.J. Morrow, G.D. Knight, T.J. Scallen, In vivo formation of 25-hydroxycholesterol from endogenous cholesterol after a single meal, dietary cholesterol challenge, J. Lipid Res. 35 (12) (1994) 2241–2253.
[66] E.M. van der Pijl, M. van Putten, E.H. Niks, J.J. Verschuuren, A. Aartsma-Rus, J. J. Plomp, Characterization of neuromuscular synapse function abnormalities in multiple Duchenne muscular dystrophy mouse models, Eur. J. Neurosci. 43 (12) (2016) 1623–1635, https://doi.org/10.1111/ejn.13249.
[67] Y. Li, Y. Lee, W.J. Thompson, Changes in aging mouse neuromuscular junctions are explained by degeneration and regeneration of muscle fiber segments at the synapse, J. Neurosci. 31 (42) (2011) 14910–14919, https://doi.org/10.1523/JNEUROSCI.3590-11.2011.
[68] E. Tremblay, E. Martineau, R. Robitaille, Opposite synaptic alterations at the neuromuscular junction in an ALS mouse model: when motor units matter, J. Neurosci. 37 (37) (2017) 8901–8918, https://doi.org/10.1523/JNEUROSCI.3090-16.2017.
[69] Y. Li, W.J. Thompson, Nerve terminal growth remodels neuromuscular synapses in mice following regeneration of the postsynaptic muscle fiber, J. Neurosci. 31 (37) (2011) 13191–13203, https://doi.org/10.1523/JNEUROSCI.2953-11.2011.
[70] M. Rich, J.W. Lichtman, Motor nerve terminal loss from degenerating muscle fibers, Neuron 3 (6) (1989) 677–688, https://doi.org/10.1016/0896-6273(89)90236-5.
[71] G. Valdez, J.C. Tapia, J.W. Lichtman, M.A. Fox, J.R. Sanes, Shared resistance to aging and ALS in neuromuscular junctions of specific muscles, PLoS One 7 (4) (2012), e34640, https://doi.org/10.1371/journal.pone.0034640.
[72] C.R. Slater, 'Fragmentation' of NMJs: a sign of degeneration or regeneration? A long journey with many junctions, Neuroscience 439 (2020) 28–40, https://doi.org/10.1016/j.neuroscience.2019.05.017.
[73] Parakh S, Spencer DM, Halloran MA, Soo KY, Atkin JD. Redox regulation in amyotrophic lateral sclerosis. Oxidative Med. Cell. Longev.. 2013;2013:408681. doi: https://doi.org/10.1155/2013/408681.
[74] A.N. Tsentsevitsky, G.F. Zakyrjanova, A.M. Petrov, Cadmium desynchronizes neurotransmitter release in the neuromuscular junction: key role of ROS, Free Radic. Biol. Med. 155 (2020) 19–28, https://doi.org/10.1016/j.freeradbiomed.2020.05.017.
[75] J. Zhai, A.L. Strom, R. Kilty, P. Venkatakrishnan, J. White, W.V. Everson, et al., Proteomic characterization of lipid raft proteins in amyotrophic lateral sclerosis mouse spinal cord, FEBS J. 276 (12) (2009) 3308–3323, https://doi.org/10.1111/j.1742-4658.2009.07057.x.
[76] J.T. Vollrath, A. Sechi, A. Dreser, I. Katona, D. Wiemuth, J. Vervoorts, et al., Loss of function of the ALS protein SigR1 leads to ER pathology associated with defective autophagy and lipid raft disturbances, Cell Death Dis. 5 (2014) e1290, https://doi.org/10.1038/cddis.2014.243.
[77] A. Antonini, S. Caioli, L. Saba, G. Vindigni, S. Biocca, N. Canu, et al., Membrane cholesterol depletion in cortical neurons highlights altered NMDA receptor functionality in a mouse model of amyotrophic lateral sclerosis, Biochim. Biophys. Acta Mol. basis Dis. 1864 (2) (2018) 509–519, https://doi.org/10.1016/j.bbadis.2017.11.008.
[78] A. Henriques, V. Croixmarie, D.A. Priestman, A. Rosenbohm, S. Dirrig-Grosch, E. D'Ambra, et al., Amyotrophic lateral sclerosis and denervation alter sphingolipids and up-regulate glucosylceramide synthase, Hum. Mol. Genet. 24 (25) (2015) 7390–7405, https://doi.org/10.1093/hmg/ddv439.
[79] A.M. Petrov, M.R. Kasimov, A.R. Giniatullin, O.I. Tarakanova, A.L. Zefirov, The role of cholesterol in the exo- and endocytosis of synaptic vesicles in frog motor nerve endings, Neurosci. Behav. Physiol. 40 (8) (2010) 894–901, https://doi.org/10.1007/s11055-010-9338-9.
[80] A.M. Petrov, G.F. Zakyrjanova, A.A. Yakovleva, A.L. Zefirov, Inhibition of protein kinase C affects on mode of synaptic vesicle exocytosis due to cholesterol depletion, Biochem. Biophys. Res. Commun. 456 (1) (2015) 145–150, https://doi.org/10.1016/j.bbrc.2014.11.049.
[81] Zamir O, Charlton MP. Cholesterol and synaptic transmitter release at crayfish neuromuscular junctions. J. Physiol.. 2006;571(Pt 1):83–99. doi: https://doi.org/10.1113/jphysiol.2005.098319.
[82] S. Sugita, L.L. Fleming, C. Wood, S.K. Vaughan, M.P. Gomes, W. Camargo, et al., VAChT overexpression increases acetylcholine at the synaptic cleft and accelerates aging of neuromuscular junctions, Skelet. Muscle 6 (2016) 31, https://doi.org/10.1186/s13395-016-0105-7.
[83] C. Pato, F. Stetzkowski-Marden, K. Gaus, M. Recouvreur, A. Cartaud, J. Cartaud, Role of lipid rafts in agrin-elicited acetylcholine receptor clustering, Chem. Biol. Interact. 175 (1–3) (2008) 64–67, https://doi.org/10.1016/j.cbi.2008.03.020.
[84] R. Willmann, S. Pun, L. Stallmach, G. Sadasivam, A.F. Santos, P. Caroni, et al., Cholesterol and lipid microdomains stabilize the postsynapse at the neuromuscular junction, EMBO J. 25 (17) (2006) 4050–4060, https://doi.org/10.1038/sj.emboj.7601288.
[85] H.L. Fernandez, J.R. Stiles, J.A. Donoso, Skeletal muscle acetylcholinesterase molecular forms in amyotrophic lateral sclerosis, Muscle Nerve 9 (5) (1986) 399–406, https://doi.org/10.1002/mus.880090504.
[86] M.T. Moral-Naranjo, M.F. Montenegro, E. Munoz-Delgado, F.J. Campoy, C. J. Vidal, Targeting of acetylcholinesterase to lipid rafts of muscle, Chem. Biol. Interact. 175 (1–3) (2008) 312–317, https://doi.org/10.1016/j.cbi.2008.04.018.
[87] R. Ursan, U.G. Odnoshivkina, A.M. Petrov, Membrane cholesterol oxidation downregulates atrial beta-adrenergic responses in ROS-dependent manner, Cell. Signal. 67 (2019), 109503, https://doi.org/10.1016/j.cellsig.2019.109503.
[88] L.S. Dantas, L.G. Viviani, A. Inague, E. Piccirillo, L. Rezende, G.E. Ronsein, et al., Lipid aldehyde hydrophobicity affects apo-SOD1 modification and aggregation, Free Radic. Biol. Med. 156 (2020) 157–167, https://doi.org/10.1016/j.freeradbiomed.2020.05.011.
[89] A.J. Brown, L.J. Sharpe, M.J. Rogers, Oxysterols: from physiological tuners to pharmacological opportunities, Br. J. Pharmacol. (2020), https://doi.org/10.1111/bph.15073.
[90] A.M. Petrov, M.R. Kasimov, A.L. Zefirov, Cholesterol in the pathogenesis of Alzheimer's, Parkinson's diseases and autism: link to synaptic dysfunction, Acta Nat. 9 (1) (2017) 26–37.
[91] W.J. Griffiths, Y. Wang, Oxysterol research: a brief review, Biochem. Soc. Trans. 47 (2) (2019) 517–526, https://doi.org/10.1042/BST20180135.
[92] J.G. Cyster, E.V. Dang, A. Reboldi, T. Yi, 25-Hydroxycholesterols in innate and adaptive immunity, Nat. Rev. Immunol. 14 (11) (2014) 731–743, https://doi.org/10.1038/nri3755.
[93] S. Lv, C. Ju, J. Peng, M. Liang, F. Zhu, C. Wang, et al., 25-hydroxycholesterol protects against myocardial ischemia-reperfusion injury via inhibiting PARP activity, Int. J. Biol. Sci. 16 (2) (2020) 298–308, https://doi.org/10.7150/ijbs.35075.
[94] A. Civra, R. Francese, P. Gamba, G. Testa, V. Cagno, G. Poli, et al., 25-Hydroxycholesterol and 27-hydroxycholesterol inhibit human rotavirus infection by sequestering viral particles into late endosomes, Redox Biol. 19 (2018) 318–330, https://doi.org/10.1016/j.redox.2018.09.003.
[95] X. Xu, E. London, The effect of sterol structure on membrane lipid domains reveals how cholesterol can induce lipid domain formation, Biochemistry 39 (5) (2000) 843–849, https://doi.org/10.1021/bi992543v.
[96] A. Goto, M. Charman, N.D. Ridgway, Protein kinase D1 and oxysterol-binding protein form a regulatory complex independent of phosphorylation, Traffic 19 (11) (2018) 854–866, https://doi.org/10.1111/tra.12609.
[97] R.J. Perry, N.D. Ridgway, Oxysterol-binding protein and vesicle-associated membrane protein-associated protein are required for sterol-dependent activation of the ceramide transport protein, Mol. Biol. Cell 17 (6) (2006) 2604–2616, https://doi.org/10.1091/mbc.e06-01-0060.
[98] E. Teuling, S. Ahmed, E. Haasdijk, J. Demmers, M.O. Steinmetz, A. Akhmanova, et al., Motor neuron disease-associated mutant vesicle-associated membrane protein-associated protein (VAP) B recruits wild-type VAPs into endoplasmic reticulum-derived tubular aggregates, J. Neurosci. 27 (36) (2007) 9801–9815, https://doi.org/10.1523/JNEUROSCI.2661-07.2007.
[99] A. Moustaqim-Barrette, Y.Q. Lin, S. Pradhan, G.G. Neely, H.J. Bellen, H. Tsuda, The amyotrophic lateral sclerosis 8 protein, VAP, is required for ER protein quality control, Hum. Mol. Genet. 23 (8) (2014) 1975–1989, https://doi.org/10.1093/hmg/ddt594.
[100] A. Darbyson, J.K. Ngsee, Oxysterol-binding protein ORP3 rescues the amyotrophic lateral sclerosis-linked mutant VAPB phenotype, Exp. Cell Res. 341 (1) (2016) 18–31, https://doi.org/10.1016/j.yexcr.2016.01.013.